Clim. Past Discuss., 8, 1885–1914, 2012
www.clim-past-discuss.net/8/1885/2012/
doi:10.5194/cpd-8-1885-2012

Climate of the Past Discussions

Modeling the climatic implications of the Guliya $\delta^{18}O$ record during the past 130 ka

D. Xiao[1], P. Zhao[2], Y. Wang[3], and X. Zhou[1,4]

[1]Chinese Academy of Meteorological Sciences, Beijing, 100081, China
[2]National Meteorological Information Center, Beijing, 100081, China
[3]State Key Laboratory of Marine Geology, Tongji University, Shanghai, 200092, China
[4]State Key Laboratory of Severe Weather, Beijing, 100081, China

Received: 29 March 2012 – Accepted: 7 May 2012 – Published: 22 May 2012

Correspondence to: P. Zhao (zhaop@cma.gov.cn)

Published by Copernicus Publications on behalf of the European Geosciences Union.

Abstract

Using an intermediate-complexity UVic Earth System Climate Model (UVic Model), the geographical and seasonal implications and an indicative sense of the historical climate found in the δ^{18}O record of the Guliya ice core (hereinafter, the Guliya δ^{18}O) are investigated under time-dependent orbital forcing with an acceleration factor of 100 over the past 130 ka. The results reveal that the simulated late-summer (August–September) Guliya surface air temperature (SAT) reproduces the 23-ka precession and 43-ka obliquity cycles in the Guliya δ^{18}O. Furthermore, the Guliya δ^{18}O is significantly correlated with the SAT over the Northern Hemisphere (NH), which suggests the Guliya δ^{18}O is an indicator of the late-summer SAT in the NH. Corresponding to the warm and cold phases of the precession cycle in the Guliya temperature, there are two anomalous patterns in the SAT and sea surface temperature (SST) fields. The first anomalous pattern shows an increase in the SAT (SST) toward the Arctic, possibly associated with the joint effect of the precession and obliquity cycles, and the second anomalous pattern shows an increase in the SAT (SST) toward the equator, possibly due to the influence of the precession cycle. Additionally, the summer (winter) Guliya and NH temperatures are higher (lower) in the warm phases of Guliya late-summer SAT than in the cold phases. Furthermore, the Guliya SAT is closely related to the North Atlantic SST, in which the Guliya precipitation may act as a "bridge" linking the Guliya SAT and the North Atlantic SST.

1 Introduction

Compared to other proxy data, ice core records offer long-time-scale, continuous, and high-resolution climatic and environmental records of many informational parameters (Yao and Wang, 1997). Since the proposal of ice core research in 1954 and the first sampling in 1966 (Dansgaard et al., 1969), ice cores have been obtained over the North and South Poles and across the middle and low latitudes, including the Vostok ice core

CPD
8, 1885–1914, 2012

in the Antarctica (Lorius et al., 1985), the Greenland GRIP (Greenland Ice-Core Project Members, 1993) and GRIP2 ice cores (Grootes et al., 1993; Taylor et al., 1993) in the Arctic, the Devon Island ice cores in Canada (Paterson et al., 1977), and the Guliya ice cores at the North Tibetan Plateau (Thompson et al., 1997; Yao et al., 1997). These ice core records have all been used to reconstruct the record of environmental changes dating to the last interglacial stage. The major climatic events over the past 130 ka include the last interglacial stage, the last glacial stage, and a new interglacial stage, viz., the Holocene (Shi et al., 2000). The environmental changes recorded by the above ice cores greatly extend our temporal range since the last interglacial stage. Recently, the climatic implications of the ice core records have been increasingly investigated.

Among the long-term ice core records, the Guliya ice core is located in a northern subtropical region and is thus helpful for understanding the effects of climate change in the middle and low latitudes. The Guliya ice cap is the largest (with a total area of 376.1 km^2), the highest (with an elevation of 6700 m), and the thickest (with an average thickness of approximately 200 m and a maximum thickness of approximately 350 m) ice body found in the middle and low latitudes of the Northern Hemisphere (NH) (Yao et al., 1994, 2000). In 1992, Chinese and American scientists drilled into the Guliya glacier in the North Tibetan Plateau at 81.5° E, 35.2° N and retrieved three ice cores with lengths of 34.5, 93.2, and 308.6 m.

The stable oxygen isotope records in these ice cores constitute reliable indicators of environmental change (Li et al., 2000). The environmental changes over the past 130 ka are recorded as fluctuations in the concentration of oxygen-18 ($\delta^{18}O$) in precipitation found in the Guliya ice core (hereinafter referred to as the Guliya $\delta^{18}O$). The observed monthly $\delta^{18}O$ in Guliya precipitation is well correlated with local the monthly surface air temperature (SAT) during the past decades (1960–1990) (Yao et al., 1996a). Therefore, the Guliya $\delta^{18}O$ record is considered to be representative of the temperature of the Tibetan Plateau (Yao et al., 1995, 1996a), which witnessed significant warm and cold periods, either in the interglacial stage or in the glacial stage, over the past 130 ka. The alternation of these warm and cold periods indicated obvious 23-ka cycles (Yao

CPD
8, 1885–1914, 2012

et al., 1997). The Guliya $\delta^{18}O$ has been used to investigate the features of the Younger Drays and Heinrich events and to compare with the Arctic and Antarctic records (Yang et al., 1997), and has also been used as a temperature index to investigate temporal structures over many periods including the orbital and sub-orbital scales, the millennial scale, the century scale, the decadal scale, and others (Yao et al., 1996b, 1997, 2001; Shi et al., 1999).

Moreover, due to the influence of precessional motion on the seasonal and latitudinal asymmetries of solar insolation (Milankovitch, 1969; Liu and Shi, 2009), the Guliya $\delta^{18}O$ may contain climate signals for a certain season and at particular latitudes. For example, the Guliya $\delta^{18}O$ record is closely related to June solar insolation at 60° N. However, June solar insolation at this latitude leads the Guliya $\delta^{18}O$ trace by approximately one-quarter phase of the precession cycle (5 ka) (Yao et al., 1997), which suggests that the Guliya $\delta^{18}O$ does not represent the June SAT.

Although the climatic implications of the Guliya $\delta^{18}O$ record have been extensively investigated, the temporal and spatial climate ranges represented by the Guliya $\delta^{18}O$ and the climatic relationship on longer timescales between the Guliya $\delta^{18}O$ and global climate change remain unclear (Zhang et al., 1995; Yao et al., 1996a). Therefore, it is important to further investigate the temporal and spatial climate ranges represented by the Guliya $\delta^{18}O$ and the indicative capacity of the Guliya $\delta^{18}O$ for the SAT and sea surface temperature (SST) during the warm and cold phases of the 23-ka precession cycle.

In the context of the Milankovitch astronomic climate theory (Milankovitch, 1969), the latitudinal and seasonal cycles of solar insolation modulated by the earth orbital parameters (precession, obliquity, and eccentricity) are the ultimate driving forces for the millennial- and orbital-scale climate changes and glacial cycles. Employing climate models to investigate the responses of the earth climate system to this orbital forcing is useful for exploring the influences of these orbital parameters. Equilibrium simulations are often used to provide "snapshots" of the equilibrium climate for a prescribed insolation or orbital parameter (Kutzbach, 1981; Hewitt and Mitchell, 1998; Montoya et al.,

CPD
8, 1885–1914, 2012

2000; Liu et al., 2006). However, such equilibrium simulations are unable to simulate the forcing effects of the varying orbital parameters on the climate system. Thus, transient simulations are employed to study the influence of varying orbital parameters on climate (Lorenz and Lohmann, 2004; Kutzbach et al., 2008).

In this study, we employ an intermediate-complexity coupled ocean-atmosphere climate model with accelerated orbital forcing to better understand the geographical and seasonal implications and the indicative properties of the Guliya δ^{18}O record with respect to the atmosphere-ocean systems at middle and low latitudes. The remainder of this paper is organized as follows. The model and methods are described in Sect. 2. The geographical and seasonal climate implications of the Guliya δ^{18}O record are modeled in Sect. 3. The SAT anomalies associated with the Guliya temperature are described in Sect. 4. The SST anomalies associated with the Guliya temperature and the SST effects on the Guliya temperature are discussed in Sect. 5. A summary and conclusions are presented in Sect. 6.

2 Model and methods

This study employs version 2.9 of the UVic Earth System Climate Model (UVic Model) with a resolution of 3.6° in longitude and 1.8° in latitude. The UVic Model is an intermediate-complexity coupled atmosphere-ocean model (Weaver et al., 2001) in which the atmospheric model comprises a single-layer energy-moisture balance model and the ocean component utilizes version 2.2 of the GFDL Modular Ocean Model with 19 vertical levels. The UVic Model can capture several major features of global surface temperature and precipitation and has been widely used in paleoclimate research (Weaver et al., 2001; Matthews et al., 2004; Stouffer et al., 2006; Weber et al., 2007; Fyke et al., 2011). Transient simulations are used to display the evolution of climate changes over time. However, it is difficult to simulate a period of one hundred thousand years using the complicated coupled models to explore climate responses to orbital forcing. Thus, integrated acceleration schemes were applied in transient paleoclimate

CPD
8, 1885–1914, 2012

simulations (Jackson and Broccoli, 2003; Timm and Timmermann, 2007; Timmermann et al., 2007; Kutzbach et al., 2008). Lorenz and Lohmann (2004) found that acceleration factors of 10 and 100 yield similar results. The used time-dependent orbital forcing (due to changes in longitude of perihelion, axial tilt and eccentricity) was calculated according to Berger (1978). The UVic Model had been run for 200 model years under the prescribed orbital forcing. Then, we accelerate the orbital forcing by a factor of 100, i.e., the orbital parameters are advanced by 100 yr at the end of each year in the simulation. The accelerated simulation runs from 130.8 ka BP to the present. The 1308 time samples (corresponding to the period from 130.8 ka BP to the present) of the model output are analyzed in this study.

The temperature over the Guliya region in the model is the averaged SAT over the region (80–85° E, 33–38° N). Because there are 1308 model years in this simulation, the Guliya δ^{18}O data obtained from Yao et al. (1997) are linearly interpolated over the 1308 model years. The smoothness of the time series of an approximately 51-yr moving mean of the Guliya δ^{18}O is similar to that of the simulated Guliya temperature. For the 51-yr moving mean time series over 1308 yr, a Monte Carlo Simulation gives the critical value of the correlation coefficient at the 95 % confidence level as 0.26. In this study, the late summer is defined as the period from August to September.

A correlation analysis was applied to examine the relation of the Guliya δ^{18}O to the simulated SAT and SST. The lagging and leading correlations were also employed to examine the relationship between the two variables. A composite analysis was used to evaluate differences in the SAT and SST during the high and low phases of the 23-ka precession cycles in the Guliya SAT. A power spectrum analysis was performed to display the periods of the Guliya δ^{18}O record using the REDFIT software in MATLAB (Schulz and Mudelsee, 2002). A squared wavelet coherence analysis (Grinsted et al., 2004) was used to determine the relative phase relationship between the Guliya temperature and the Guliya δ^{18}O.

CPD
8, 1885–1914, 2012

3 Temporal and spatial climatic implications of the Guliya δ^{18}O

It is known that the Guliya δ^{18}O experienced several approximately 23-ka cycles in the past 130 ka that are directly related to varying earth orbital parameters (Yao et al., 1997). However, the solar insolation differs over the twelve months of the year due to precessional motion. Thus, we first examine the climate implications of the Guliya δ^{18}O.

Figure 1 presents the annual cycles of the simulated SAT anomalies over the Guliya region over the past 130 ka. In this figure, the annual cycle of SAT anomalies is composed of approximately eleven vertical belts toward the right, with lifetimes similar to the 23-ka precession cycle, and the variability of the SAT anomalies is dominant in April to August, with the largest value generally observed in June. The June SAT anomalies vary in magnitude by approximately 6 °C. These results indicate that the distributions of solar insolation and SAT anomalies differ over the twelve months of a year.

Because June insolation at 60° N is approximately one-quarter phase ahead of the Guliya δ^{18}O (Yao et al., 1997), the phases of the precession cycle in the July–December temperature may be ahead of or synchronous with the variation in the Guliya δ^{18}O. Here, we examine the relationship between the Guliya δ^{18}O and the simulated Guliya SAT in June–December. Figure 2 presents the correlation coefficients between the Guliya δ^{18}O and the simulated Guliya SAT. We observed positive correlation coefficients of 0.43 in August and 0.4 in September that are both significant at the 99 % confidence level. Figure 3 further illustrates the distribution of correlation coefficients between the Guliya δ^{18}O and the simulated late-summer SAT. Here, significant positive correlation coefficients cover the majority of the NH and exceed 0.48 at latitudes of 45°–80° N. Figure 4 presents the time series of the Guliya δ^{18}O and the simulated late-summer Guliya SAT. Both clearly present an approximately 23-ka precession cycle and show an in-phase relationship during the majority of the studied time period, except for 45–20 ka, with a positive correlation coefficient of 0.47 (exceeding the 99.9 % confidence level). The power spectrum of the Guliya δ^{18}O reveals the presence of

CPD
8, 1885–1914, 2012

two significant periods at 43.6 ka and 20.762 ka and a peak of red noise at 10.634 ka (Fig. 5). It is evident that the two significant periods correspond to the periods of the precession and the obliquity, respectively, which indicates that the Guliya δ^{18}O was mainly modulated by precessional motion and obliquity variation over the past 130 ka. The simulated Guliya SAT displays two main periods at 43.599 ka and 22.947 ka and a peak of red noise at 11.179 ka (Figure not shown), in which the precession period at 22.947 ka is more significant than the obliquity period. It can be seen that our simulation is able to successfully capture the main periods of the Guliya δ^{18}O. Figure 6 displays the squared wavelet coherence between the Guliya δ^{18}O and the simulated late-summer Guliya SAT. The precession and obliquity cycles in the Guliya δ^{18}O are manifested in the Guliya SAT as wavelengths of approximately 23 ka and 43 ka because the arrows at these periods generally point toward to the right, which indicates in-phase relationships between the simulated Guliya SAT and the Guliya δ^{18}O in both the 23-ka precession cycle and the 43-ka obliquity cycle. In the 23-ka period, the arrows deflect downward (indicating a phase angle less than 90°) during the 45–20 ka BP (Fig. 6) that correspond to the fifth peak of the Guliya δ^{18}O in Fig. 4, which indicates that the simulated Guliya SAT and the Guliya δ^{18}O are not in phase during this period. These results suggest that the Guliya δ^{18}O record generally represents the precession and obliquity cycles and their in-phase relationships over the past 130 ka, and represents the late-summer temperature not only over the Tibetan Plateau and its adjacent areas but also over the NH.

4 SAT anomalies associated with the Guliya temperature

As shown in Fig. 4, warm phases in the simulated late-summer Guliya temperatures occur at 11–6, 33–28, 59–54, 83–78, and 105–100 ka BP, while cool phases occur at 23–18, 45–40, 72–67, 94–89, and 117–112 ka BP. Based on these selected warm and cool phases, we examined variations of the SAT in the 23-ka cycle using a composite analysis.

CPD
8, 1885–1914, 2012

Figure 7a displays the composite difference of the simulated late-summer SATs between 11–6 ka BP and 23–18 ka BP (11–6 ka BP minus 23–18 ka BP), which corresponds to the difference between the early Holocene and the Last Glacial Maximum. Compared with the cold phase in 23–18 ka BP, the SAT in the warm phase during 11–6 ka BP is significantly warmer over the NH middle and lower latitudes, and large temperature anomalies occur over the Asian and African continents, with a maximum value of approximately 1.4 °C. The temperature anomalies over the Southern Hemisphere (SH) and the ocean are weaker than those over the NH and land. The anomalies generally increase toward the Arctic. A similar anomalous pattern also occurs between 59–54 ka BP and 72–67 ka BP (Fig. 7c), and between 105–100 ka BP and 117–112 ka BP (Fig. 7e); that is, there are higher (lower) temperature anomalies over the NH (SH) when the late-summer Guliya SAT is high.

However, another anomalous pattern in the SAT also occurs between the high and low late-summer Guliya SAT cases. Figure 7b presents the composite difference in the SATs between 33–28 ka BP and 45–40 ka BP. In this figure, the SAT anomalies generally show an increase toward the equator, and relative to 45–40 ka BP, the SAT in the 33–28 ka BP period was warmer over the majority of regions except the NH high latitudes, with anomalous warm centers above 1.2 °C in Africa and South America. A similar anomalous pattern is also observed in Fig. 7d. This result reveals the presence of different anomalous patterns associated with the Guliya temperature during the warm and cool phases of the precession cycle. Why do these two anomalous SAT patterns occur?

As the obliquity cycle significantly modulates the earth's climate (Short et al., 1991), especially at high latitudes, and is more evident in the Arctic, we compare the temporal evolutions of the Arctic and the Guliya SATs in an attempt to understand the contributions of the precession and obliquity cycles to the two anomalous patterns between the warm and cold phases. Figure 8 shows the simulated temporal curves for the Arctic (0–360°, 80–90° N) SAT and the Guliya SAT during the past 130 ka. The Arctic air temperature displays both the 43.6-ka obliquity and 21.8-ka precession cycles, and the

CPD
8, 1885–1914, 2012

former is more significant than the latter (Figure not shown). Thus, the Arctic temperature may well reflect an obliquity influence. As illustrated in Fig. 8, the warm and cold phases of the precession cycle in the Guliya temperature, associated with the first type of anomalous SAT pattern, are generally superposed on those of the obliquity cycle in the Arctic temperature, while the warm and cold phases of the precession cycle in the Guliya temperature, associated with the second type of anomalous SAT pattern, are not superposed on those of the obliquity cycles in the Arctic temperature. Therefore, the occurrence of two anomalous patterns in the SAT may be associated with the superposition of the precession cycle and the obliquity cycle. Specifically, the first anomalous SAT pattern is influenced both by the precession and obliquity cycles, and the second anomalous SAT pattern is mainly influenced by the precession cycle.

Figure 9 presents the annual cycles of the modeled Guliya SAT for five warm and cold phases and their differences. It appears that the annual cycles show similar features for each warm and cold phase, with the highest temperatures in June and July and the lowest temperatures in December and January. Compared with the cold phases, the Guliya temperature during the warm phases is generally higher in the warm season (May–September) and lower in the cold season (October–April) (Fig. 9a, c–e), which indicates a larger seasonal variation in the warm phases than in the cold phases. For example, the annual ranges of July (January) temperatures between the warm and cold phases varied from 0.5 (0) °C (Fig. 9b) to 4 (2) °C (Fig. 9e). These results also exhibit a larger temperature difference between the warm and cold phases in summer than in winter. Moreover, the difference of the annual cycles in the Guliya SAT between the warm and cold phases in the late-summer Guliya SAT shows the similar feature (Fig. 9), which indicates no obvious influence of the obliquity cycle on the annual cycles in the Guliya SAT. Further analysis reveals that the NH temperature displays similarly varying features. Therefore, the warm-season (cold-season) Guliya and NH temperatures are higher (lower) in the warm phases than in the cold phases.

CPD
8, 1885–1914, 2012

5 SST anomalies associated with the Guliya temperature

Similar to the SAT, the SST anomalies between the warm and cold phases also show two different features. One occurs between 11–6 ka BP and 23–18 ka BP (Fig. 10a), between 59–54 ka BP and 72–67 ka BP (Fig. 10c), and between 105–100 ka BP and 117–112 ka BP (Fig. 10e). This pattern is characterized by a warmer NH ocean and a cooler SH ocean with SSTs increasing toward the Arctic. Another feature occurs between 33–28 ka BP and 45–40 ka BP (Fig. 10b) and between 83–78 ka BP and 94–89 ka BP (Fig. 10d), with a warmer SST at the middle and low latitudes and a cooler SST near the high latitude, which indicate increasing SSTs toward the equator. The alternation of two anomalous SST patterns also displays an approximately 43-ka obliquity cycle. Similar to the cause of the anomalous patterns in the SAT field, the first anomalous SST pattern shows contributions of both the precession and obliquity cycles, while the second anomalous SST pattern is mainly influenced by the precession cycle.

Figure 11 presents the correlation coefficients between the Guliya δ^{18}O and the SST in the late summer over the past 130 ka. Here, significant positive correlation coefficients mainly appear in the North Atlantic, the Bering Sea, the Bay of Alaska, and the Arctic region to the north of Europe, with the maximum correlation coefficient exceeding 0.57 in the North Atlantic. These results suggest a close link between the Guliya temperature and the NH (particularly the Atlantic) SST in the past 130 ka.

How do the SST anomalies associated with the late-summer Guliya SAT evolve? Figure 12a presents the leading and lagging correlation coefficients between the Guliya temperature and the North Atlantic SST. The Guliya temperature lags the North Atlantic SST by 2.5 ka (Fig. 12a), which possibly indicates an effect of the North Atlantic SST on the Guliya temperature. What physical processes are possibly responsible for this influence? One explanation is given below.

Because the δ^{18}O variable is present in the local precipitation, the Guliya precipitation may be closely related to the local temperature. Figure 13 illustrates the simulated

CPD
8, 1885–1914, 2012

late-summer SAT and precipitation curves in the Guliya region. Both precipitation and SAT display significant cycles of approximately 23 ka, and there is an out-of-phase relationship between precipitation and SAT, with a correlation coefficient of −0.95. All the peaks (valleys) in precipitation correspond to valleys (peaks) in SAT. Moreover, the variation of late-summer SAT generally lags by 1 ka relative to that of late-summer precipitation (Fig. 12b), demonstrating that the Guliya late-summer precipitation leads the Guliya temperature. Several prior studies have shown that the summer North Atlantic SST modulates atmospheric circulation over the NH and affects Asian precipitation on the decadal or longer time scales (Sutton and Hodson, 2005; Dong et al., 2006; Wang et al., 2009; Feliks et al., 2011). Therefore, the anomalous signal from the North Atlantic SST may be reflected in the Guliya precipitation record and thus affect the Guliya SAT. Such an effect leads to a close link between the Guliya SAT and the North Atlantic SST, in which the Asian precipitation may act as a "bridge" linking the North Atlantic SST and the Guliya temperature.

6 Summary and conclusion

We employed the UVic Model with accelerated orbital forcing by a factor of 100 to examine the climate implications and indicative nature of the Guliya δ^{18}O record for the past 130 ka. The simulated late-summer (August–September) Guliya temperature effectively captures the variation and the major periods of the Guliya δ^{18}O including the 43-ka obliquity and 23-ka precession cycles, with a correlation coefficient of 0.47 between the Guliya δ^{18}O and the modeled late-summer Guliya temperature. The Guliya δ^{18}O is also significantly correlated with the simulated NH late-summer SAT. Thus, the Guliya δ^{18}O record represents the temperature not only over the Tibetan Plateau but also over the NH.

Epochal differences between the warm and cold phases of the Guliya air temperature indicate two types of anomalous patterns in the SAT and SST fields. One pattern shows an increase in the SAT toward the Arctic, possibly associated with the joint influence of

CPD
8, 1885–1914, 2012

the precession and obliquity cycles, and another pattern shows an increase toward the equator, possibly attributed to the precession cycle. In the annual cycles, the Guliya and NH summer (winter) temperatures are warmer (cooler) in the warm phases of Guliya late-summer SAT than in the cold phases and the influence of the obliquity cycle on the annual cycles in the Guliya temperature is not significant.

Moreover, the Guliya temperature is closely related to the North Atlantic SST, lags the North Atlantic SST by approximately 2.5 ka, and lags the Guliya precipitation by 1 ka. These results suggest an effect of the North Atlantic SST on Asian precipitation and then on the Guliya temperature. Thus, the Guliya precipitation may be a "bridge" connecting the local temperature with the North Atlantic SST. Because the UVic Model does not exhibit atmospheric vertical circulation features, studies using a more complex coupled ocean-land-atmosphere model are required in the future.

Acknowledgements. We thank Prof. Tandong Yao for providing the Guliya ice core data and Dr. Ge Liu for using the software in MATLAB. This work was supported by a major project of the NSFC (40894050), Special Foundation for National Science and Technology Major Project of China (2011FY120300).

References

Berger, A.: Long-term variations in daily insolation and quaternary climate changes, J. Atmos. Sci., 35, 2362–2367, 1978.

Dansgaard, W., Johnson, S., Meller, J., and Langway, C. C.: One thousand centuries of climatic record from Camp Century on the Greenland ice sheet, Science, 166, 377–381, 1969.

Dong, B., Sutton, R. T., and Scaife, A. A.: Multidecadal modulation of El Niño-Southern Oscillation (ENSO) variance by Atlantic Ocean sea surface temperatures, Geophys. Res. Lett., 33, L08705, doi:10.1029/2006GL025766, 2006.

Feliks, Y. M., Ghil, M., and Robertson, A. W.: The atmospheric circulation over the North Atlantic as induced by the SST field, J. Climate, 24, 522–542, 2011.

CPD
8, 1885–1914, 2012

Fyke, J. G., Weaver, A. J., Pollard, D., Eby, M., Carter, L., and Mackintosh, A.: A new coupled ice sheet/climate model: description and sensitivity to model physics under Eemian, Last Glacial Maximum, late Holocene and modern climate conditions, Geosci. Model Dev., 4, 117–136, doi:10.5194/gmd-4-117-2011, 2011.

Greenland Ice-Core Project Members: climate instability during the last interglacial period recorded in the GRIP ice core, Nature, 364, 203–207, 1993.

Grinsted, A., Moore, J. C., and Jevrejeva, S.: Application of the cross wavelet transform and wavelet coherence to geophysical time series, Nonlin. Processes Geophys., 11, 561–566, doi:10.5194/npg-11-561-2004, 2004

Grootes, P. M., Stuiver, M., White, W. C., Johnsen, S., and Jouzel, J.: Comparison of oxygen isotope records from the GISP2 and GRIP Greenland ice cores, Nature, 366, 552–554, 1993.

Hewitt, C. and Mitchell, J.: A fully coupled general circulation model simulation of the climate of the mid-Holocene, Geophys. Res. Lett., 25, 361–364, 1998.

Jackson, C. S. and Broccoli, A. J.: Orbital forcing of Arctic climate: mechanisms of climate response and implications for continental glaciation, Clim. Dynam., 21, 539–557, 2003.

Kutzbach, J. E.: Monsoon climate of the early Holocene: Climate experiment with the Earth's orbital parameters for 9000 years ago, Science, 214, 59–61, 1981.

Kutzbach, J. E., Liu, X. D., and Liu, Z. Y.: Simulation of the evolutionary response of global summer monsoons to orbital forcing over the past 280,000 years, Clim. Dynam., 30, 567–579, 2008.

Li, Z. Q., Sun, J. Y., Hou, S. G., Tian, L. D., and Liu, B. Z.: Glaciochemistry and its environmental significance, in: Glaciers and Their Environments in China – the Present, Past and Future, edited by: Shi, Y. F., Science Press, Beijing, 411, 132–160, 2000.

Liu, X. D. and Shi, Z. G.: Effect of precession on the Asian summer monsoon evolution: a systematic review, Chinese Sci. Bull., 54, 3720–3730, doi:10.1007/s11434-009-0540-5, 2009.

Liu, Z., Wang, Y., Gallimore, R., Notaro, M., and Prentice, I. C.: On the cause of abrupt vegetation collapse in North Africa during the Holocene: climate variability vs. vegetation feedback, Geophys. Res. Lett., 33, L22709, doi:10.1029/2006GL028062, 2006.

Lorenz, S. J. and Lohmann, G.: Accelerated technique for Milankovitch type forcing in a coupled atmosphere-ocean circulation model: method and application for the Holocene, Clim. Dynam., 23, 727–743, 2004.

CPD
8, 1885–1914, 2012

Lorius, C., Jouzel, J., Ritz, C., Merlivat, L., and Barkov, N. I.: A 150 000 year climatic record from Antarctic ice, Nature, 316, 591–596, 1985.
Matthews, H. D., Weaver, A. J., Meissner, K. J., Gillett, N. P., and Eby, M.: Natural and anthropogenic climate change: incorporating historical land cover change, vegetation dynamics and the global carbon cycle, Clim. Dynam., 22, 461–479, 2004.
Milankovitch, M.: Canon of insolation and the ice-age problem (Beograd Koniglidh Serbische Akademie, 1941), English translation by the Israel program for scientific translations, US department of Commerce and National Science Foundation, Washington DC, 633 pp., 1969.
Montoya, M., von Storch, H., and Crowley, T.: Climate simulation for 125,000 years ago with a coupled ocean-atmosphere generalcirculation model, J. Climate, 13, 1057–1072, 2000.
Paterson, W. S. B., Koerner, R. M., and Fisher, D.: An oxygen-isotope climatic record from the Devon Island ice cap, Arctic Canada, Nature, 266, 508–511, 1977.
Schulz, M. and Mudelsee, M.: REDFIT: Estimating red-noise spectra directly from unevenly spaced paleoclimatic time series, Comput. Geosci., 28, 421–426, 2002.
Shi, Y. F., Yao, T. D., and Yang, B.: Decadal climatic variations recorded in Guliya ice core and comparison with the historical documentary data from East China during the last 2000 years, Sci. China, Ser. D, 29, 79–86, 1999.
Shi, Y. F., Zheng, B. X., and Su, Z.: Glaciations, glacial-interglacial cycles and environmental changes in the quaternary, in: Glaciers and Their Environments in China – the Present, Past and Future, edited by: Shi, Y. F., Science Press, Beijing, 411, 320–355, 2000.
Short, D. A., Mengel, J. G., and Crowley, T. J.: Filtering of Milankovitch cycles by Earth's geography, Quaternary Res., 35, 157–173, 1991.
Stouffer, R. J., Yin, J., Gregory, J. M., Dixon, K. W., Spelman, M. J., Hurlin, W., Weaver, A. J., Eby, M., Flato, G. M., Hasumi, H., Hu, A., Jungclause, J. H., Kamenkovich, I. V., Levermann, A., Montoya, M., Murakami, S., Nawrath, S., Oka, A., Peltier, W. R., Robitaille, D. Y., Sokolov, A., Vettoretti, G., and Weber, S. L.: Investigating the causes of the response of the thermohaline circulation to past and future climate changes, J. Climate, 19, 1365–1387, 2006.
Sutton, R. T. and Hodson, D. L. R.: Atlantic Ocean forcing of North American and European summer climate, Science, 309, 115–118, 2005.
Taylor, K. C., Hammer, C. U., Alley, R. B., Clausen, H. B., Dahl-Jensen, D., Gow, A. J., Gundestrup, N. S., Klpfstuhl, J., Moore, J. C., and Waddington, E. D.: Electrical conductivity measurements from the GISP2 and GRIP Greenland ice cores, Nature, 366, 549–552, 1993.

CPD
8, 1885–1914, 2012

Thompson, L. G., Yao, T., Davis, M. E., Henderson, K. A., Thompson, E. M., Lin, P.-N., Beer, J., Synal, H.-A., Cole-Dai, J., and Bolzan, J. F.: Tropical climate instability: the last glacial cycles from a Qinghai Tibetan ice core, Science, 276, 1821–1825, 1997.

Timm, O. and Timmermann, A.: Simulation of the last 21 000 years using accelerated transient boundary conditions, J. Climate, 20, 4377–4401, 2007.

Timmermann, A., Lorenz, S. J., An, S. I., Clement, A., and Xie, S. P.: The effect of orbital forcing on the mean climate and variability of the tropical Pacific, J. Climate, 20, 4147–4159, doi:10.1175/jcli4240.1, 2007.

Wang, Y., Li, S., and Luo, D.: Seasonal response of Asian monsoonal climate to the Atlantic Multidecadal Oscillation, J. Geophys. Res., 114, D02112, doi:10.1029/2008JD010929, 2009.

Weaver, A. J., Eby, M., Wiebe, E. C., Bitz, C. M., Duffy, P. B., Ewen, T. L., Fanning, A. F., Holland, M. M., MacFadyen, A., Matthews, H. D., Meissner, K. J., Saenko, O., Schmittner, A., Wang, H., and Yoshimori, M.: The UVic earth system climate model: model description, climatology, and applications to past, present and future climates, Atmos. Ocean, 39, 1–68, 2001.

Weber, S. L., Drijfhout, S. S., Abe-Ouchi, A., Crucifix, M., Eby, M., Ganopolski, A., Murakami, S., Otto-Bliesner, B., and Peltier, W. R.: The modern and glacial overturning circulation in the Atlantic ocean in PMIP coupled model simulations, Clim. Past, 3, 51–64, doi:10.5194/cp-3-51-2007, 2007.

Yang, Z. H., Yao, T. D., Huang, C. L., and Sun, W. Z.: Younger Drays record in the Guliya ice core, Chinese Sci. Bull., 42, 1975–1978, 1997.

Yao, T. D. and Wang, N. L.: Past, now and future of the ice core study, Chinese Sci. Bull., 42, 225–230, 1997.

Yao, T. D., Jiao, K. Q., Li, Z. Q., Shi, W. L., Li, Y. F., Liu, J. S., Huang, C. L., and Xie, C.: Climatic and environmental records in Guliya Ice Cap, Sci. China Ser. D, 37, 766–773, 1994.

Yao, T. D., Thompson, L. G., and Jiao, K. Q.: Recent warming as recorded in the Qinghai-Tibetan cryosphere, Ann. Glaciol., 21, 196–200, 1995.

Yao, T. D., Lonnie, G., Thompson, E. M., Yang, Z., Zhang, X., and Lin, P. N.: Climatological significance of δ^{18}O in the North Tibetan ice cores, J. Geophys. Res., 101, 29531–29537, 1996a.

Yao, T. D., Qin, D. H., Tian, L. D., Jiao, K. Q., Yang, Z. H., and Xie, C.: Variations in temperature and preipitation in the past 2000 years on the Xizang (Tibet) Plateau – Guliya ice core record, Sci. China Ser. D, 26, 348–353, 1996b.

CPD
8, 1885–1914, 2012

Yao, T. D., Thompson, L. G., Shi, Y. F., Qin, D. H., Jiao, K. Q., Yang, Z. H., Thompson, E. M., and Tian, L. D.: Climate variation since the last interglaciation recorded in the Guliya ice core, Sci. China Ser. D, 40, 447–452, 1997.

Yao, T. D., Wang, N. L., and Shi, Y. F.: Climate and entironmental changes recorded in the ice cores, in: Glaciers and Their Environments in China – the Present, Past and Future, edited by: Shi, Y. F., Science Press, Beijing, 411, 285–319, 2000.

Yao, T. D., Xu, B. Q., and Pu, J. C.: Climatic changes on orbital and sub-orbital time scale recorded by the Guliya ice core in Tibetan Plateau, Sci. China Ser. D, 31, 287–294, 2001.

Zhang, X., Shi, Y. F., and Yao, T. D.: Variational features of precipitation δ^{18}O in Northeast Qinghai-Tibet Plateau, Sci. China Ser. D, 25, 540–547, 1995.

CPD
8, 1885–1914, 2012

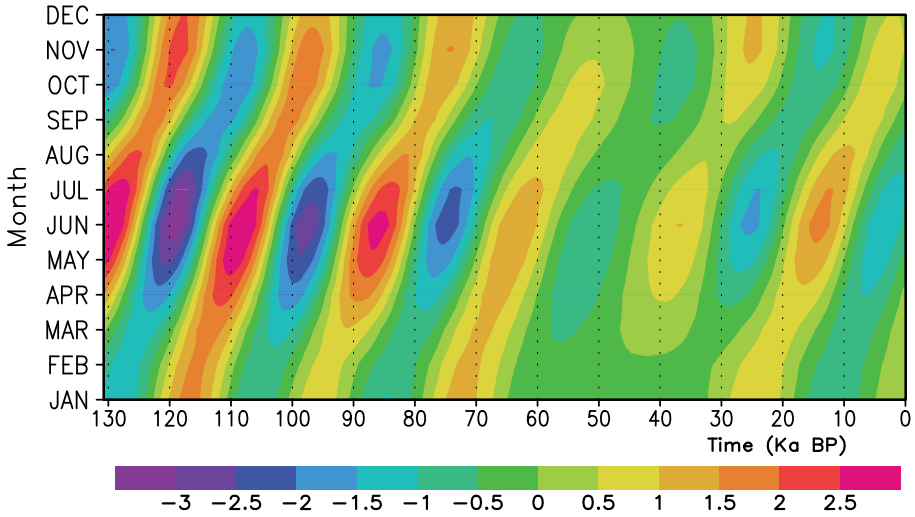

Fig. 1. Annual cycles of the simulated Guliya SAT anomalies relative to the climatological mean over the past 130 ka. The abscissa is time before the present, and the ordinate is the month of a year.

CPD
8, 1885–1914, 2012

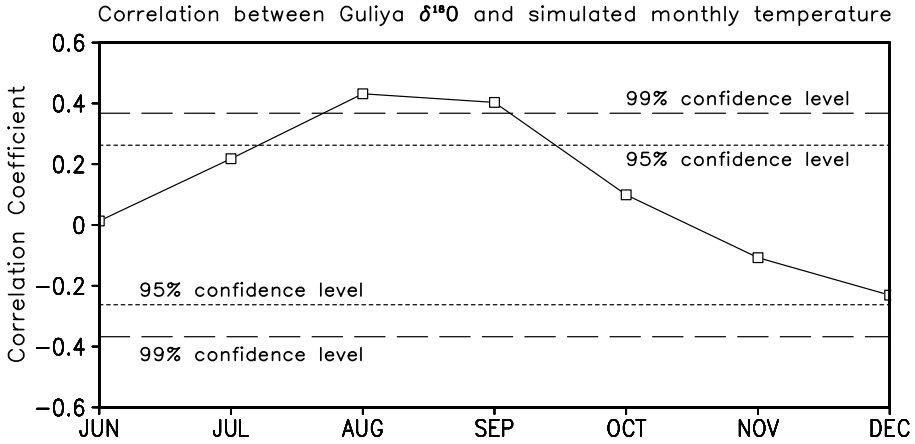

Fig. 2. Correlation coefficients (open squares) between the Guliya δ^{18}O and the simulated Guliya monthly mean SAT during the 1308 model years. The horizontal short-dashed and long-dashed lines indicate the 95 % and 99 % confidence levels, respectively.

CPD
8, 1885–1914, 2012

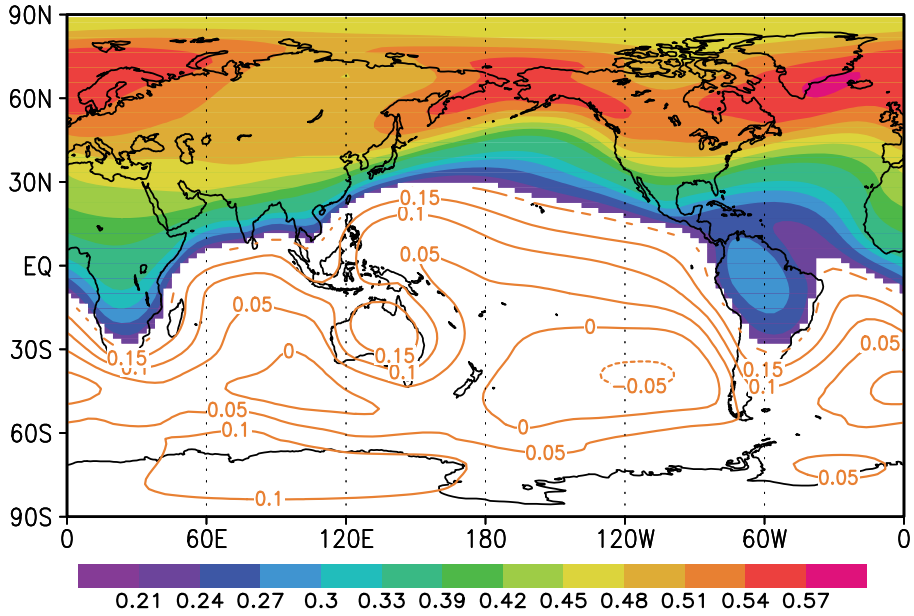

Fig. 3. Correlation coefficients between the Guliya δ^{18}O and the simulated late-summer SAT during the 1308 model years. The shading indicates the correlation coefficients significant at the 95 % confidence level, and the contours do not exceed the 95 % confidence level.

CPD
8, 1885–1914, 2012

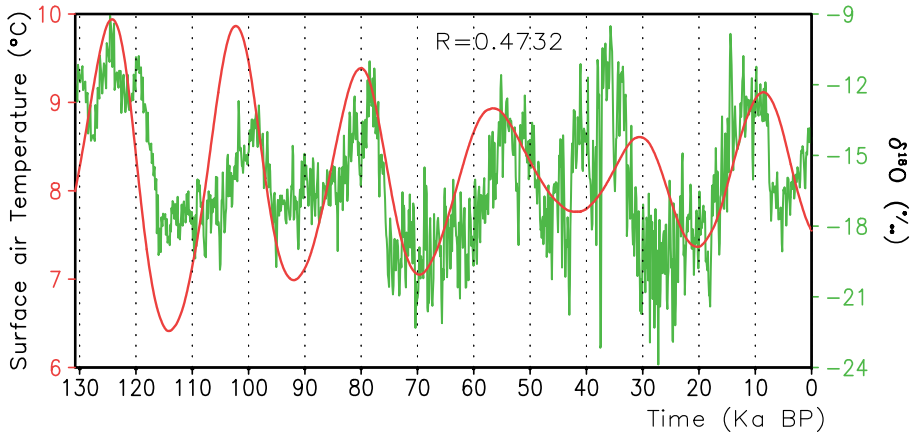

Fig. 4. Time series of the simulated Guliya late-summer SAT (red line, left ordinate) and the Guliya δ^{18}O (green line, right ordinate). The correlation coefficient (R) between them is 0.4732, significant at the 99.9 % confidence level.

CPD
8, 1885–1914, 2012

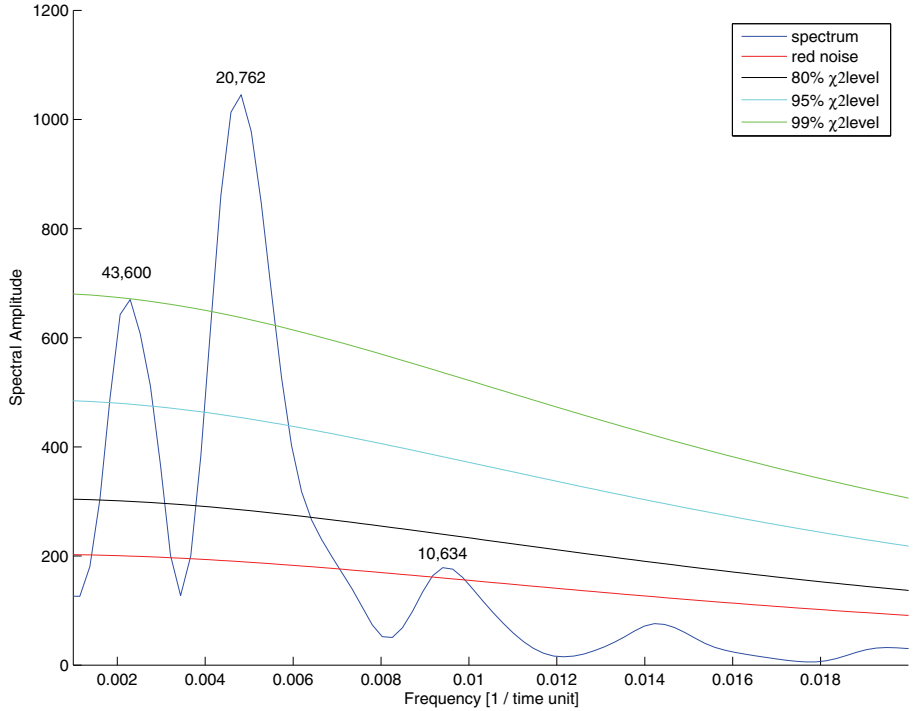

Fig. 5. Power spectrum of the Guliya δ^{18}O.

CPD
8, 1885–1914, 2012

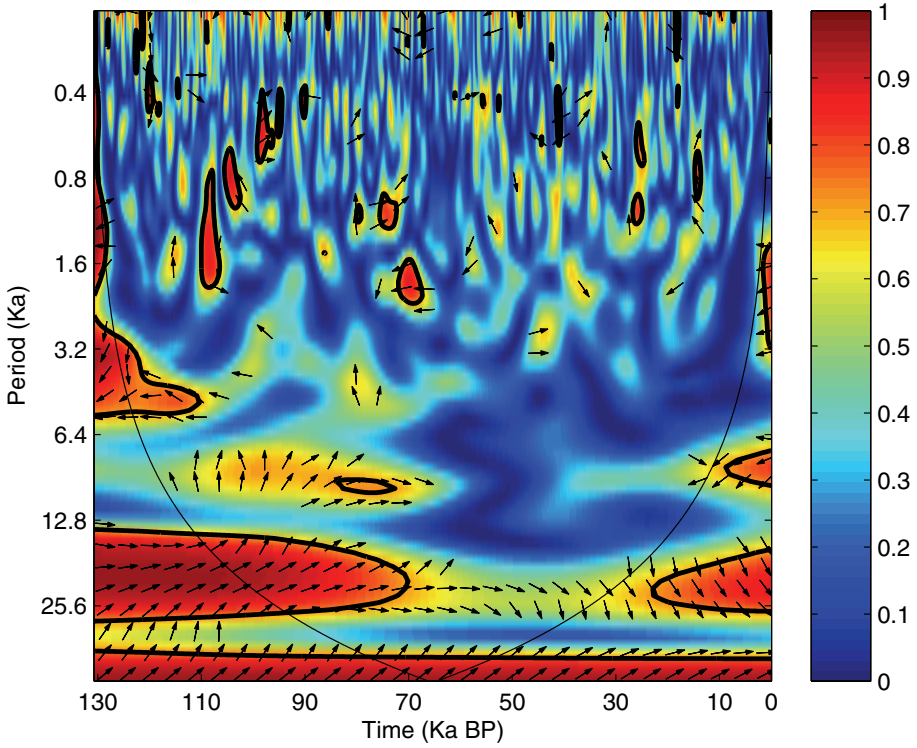

Fig. 6. Squared wavelet coherence between the simulated late-summer Guliya SAT and the Guliya δ^{18}O. The 5 % significance level against red noise is shown as a thick contour. The relative phase relationships are indicated by arrows (with in-phase pointing right, anti-phase pointing left).

CPD
8, 1885–1914, 2012

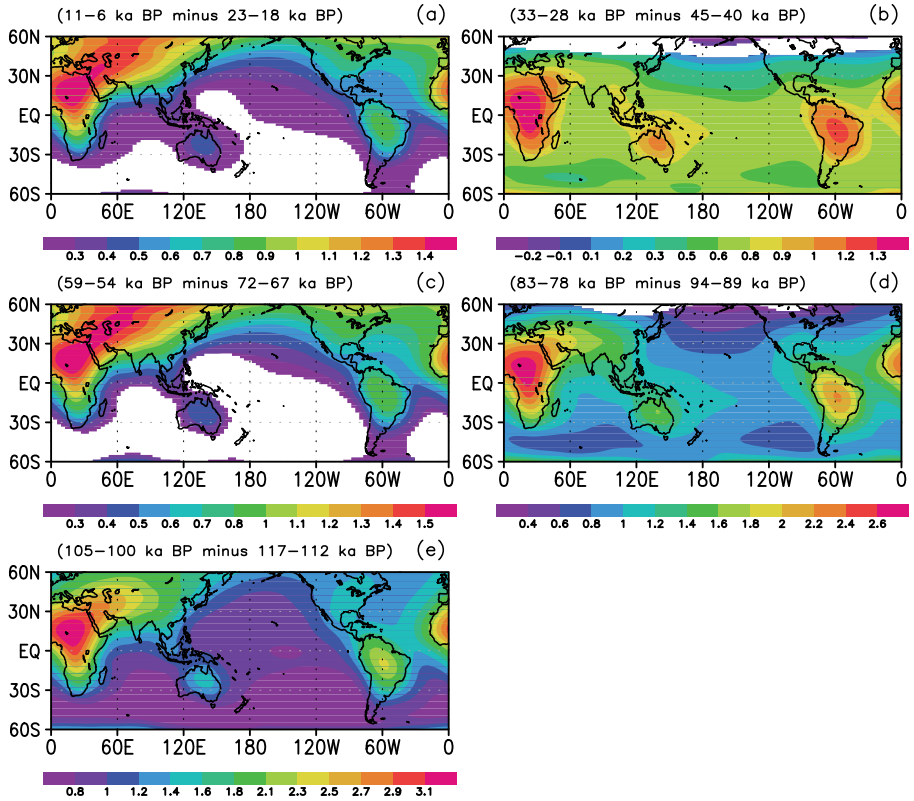

Fig. 7. Composite differences in the simulated late-summer SAT between the high and low Guliya late-summer SATs. The times of the high and low phases are indicated above each panel. The shaded areas represent the values of air temperature anomalies that are significant at the 95 % confidence level.

CPD
8, 1885–1914, 2012

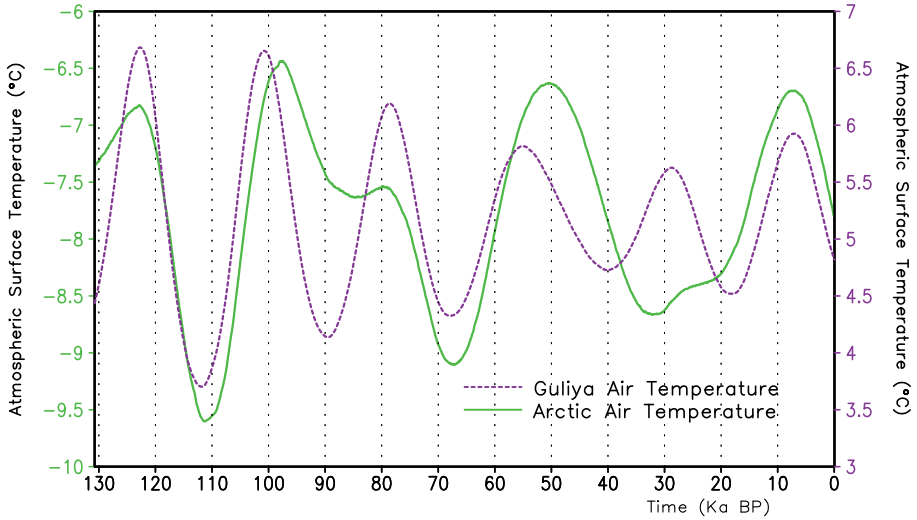

Fig. 8. Simulated late-summer Guliya (purple, right ordinate) and Arctic SATs (green, left ordinate).

CPD
8, 1885–1914, 2012

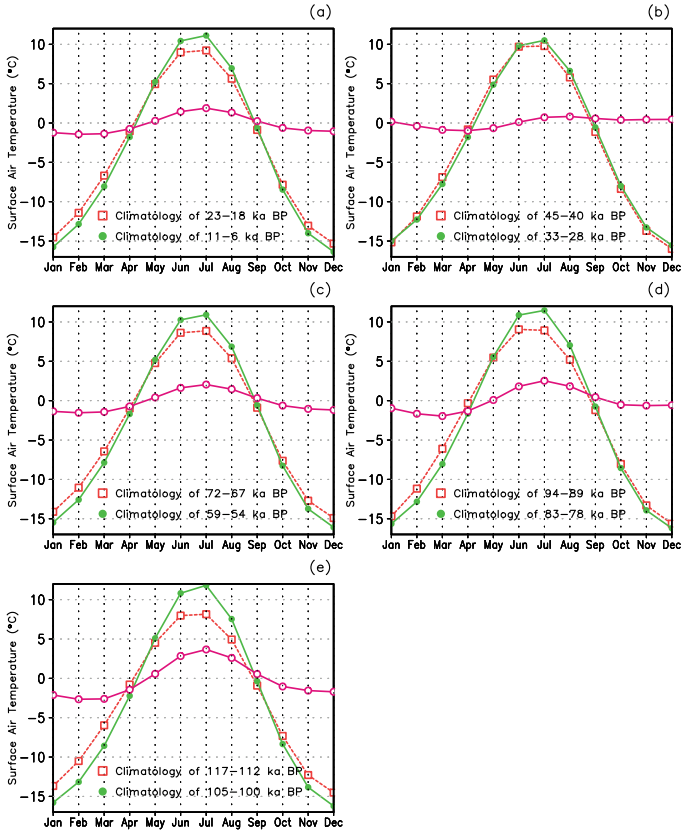

Fig. 9. Annual cycles of the Guliya SAT in the warm (closed circles) and cold phases (open squares) of the late-summer Guliya SAT and their difference (warm phase minus cold phase, open circle). The time of the warm and cold phases is indicated in each panel.

CPD
8, 1885–1914, 2012

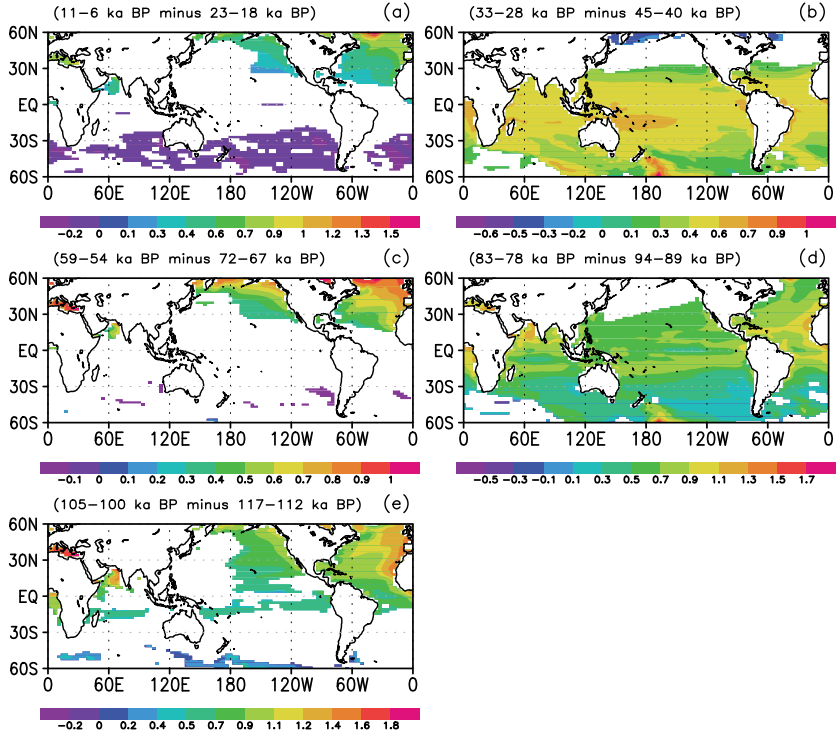

Fig. 10. Same as in Fig. 7 but for SST.

CPD
8, 1885–1914, 2012

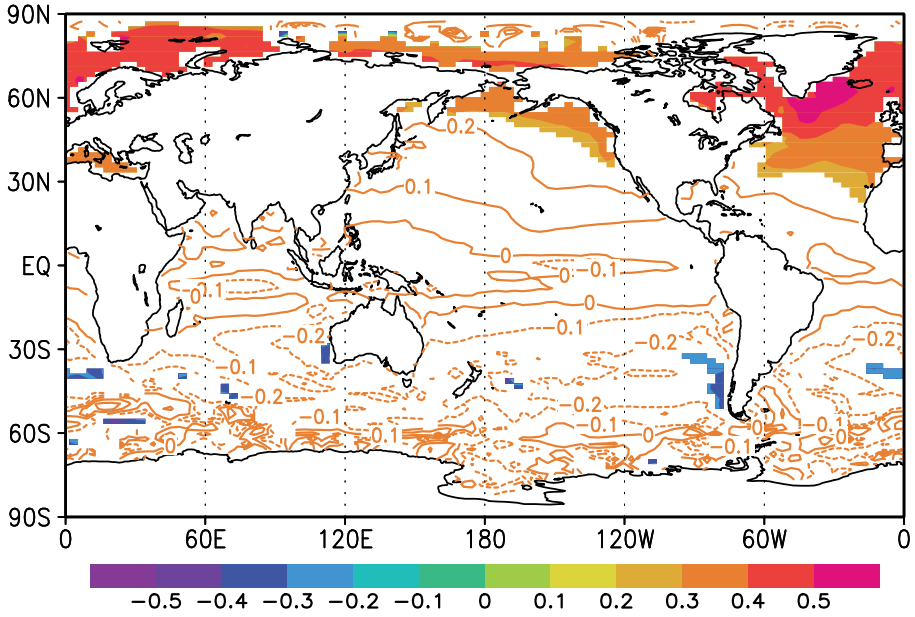

Fig. 11. Same as in Fig. 3 but for the correlation between the Guliya δ^{18}O and the simulated SST.

CPD
8, 1885–1914, 2012

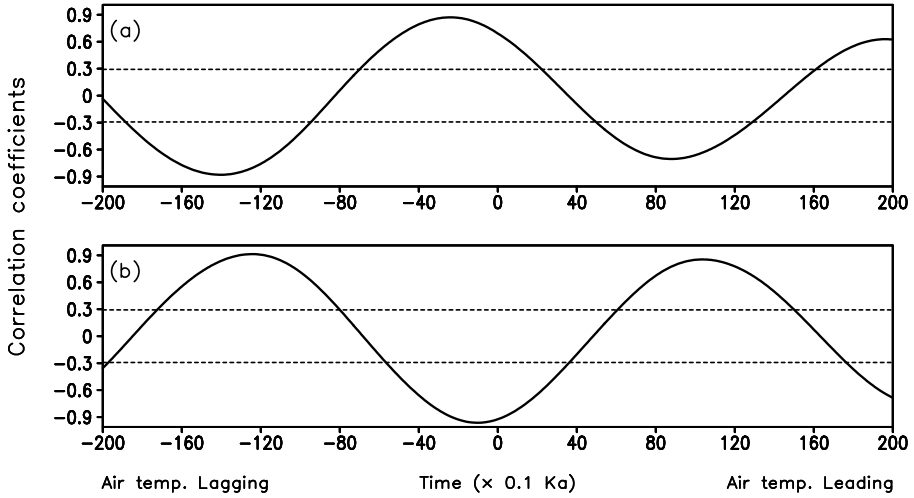

Fig. 12. Leading and lagging correlation coefficients (solid lines) between the Guliya SAT and **(a)** the North Atlantic (60–0° W, 50–70° N) SST and **(b)** the Guliya precipitation. The horizontal short-dashed lines represent the 95 % confidence level.

CPD
8, 1885–1914, 2012

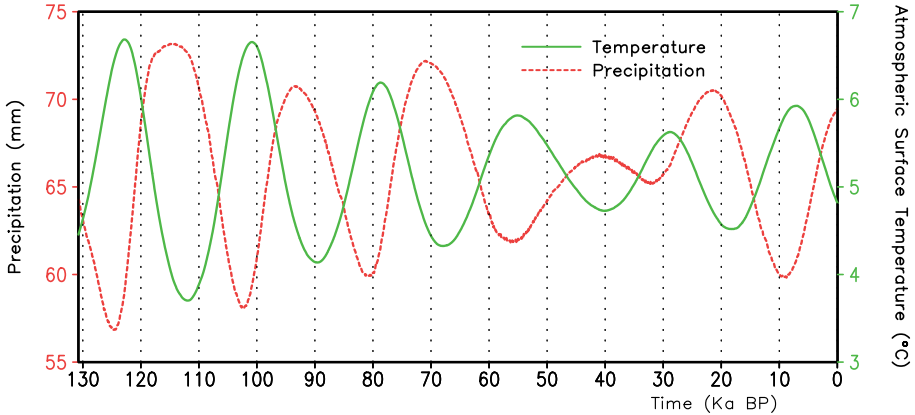

Fig. 13. The simulated late-summer Guliya SAT (green, right ordinate) and precipitation (red, left ordinate).

CPD
8, 1885–1914, 2012